Automatic Detection of Trees using Airborne LiDAR Data Based on Geometric Characteristics

Renato César dos Santos [1], Matheus Ferreira da Silva [2], Cleber Junior Alencar [3], Mauricio Galo [1]

[1] São Paulo State University – UNESP, Dept. of Cartography, Presidente Prudente, São Paulo, Brazil – renato.cesar@unesp.br, mauricio.galo@unesp.br

[2] São Paulo State University – UNESP, Graduate Program in Cartographic Sciences, Presidente Prudente, São Paulo, Brazil – matheus-ferreira.silva@unesp.br

[3] Droneng Drones e Engenharia, Presidente Prudente, São Paulo, Brazil – cleber.alencar@unesp.br

Keywords: Urban Forests, Tree Extraction, LASER Scanning, 3D Point Cloud, Photogrammetry, Remote Sensing.

Abstract

One of the essential factors in analyzing urban environments is the presence of trees. Thus, the development of automatic or semi-automatic tree detection strategies is important for monitoring and providing data for municipal authorities’ planning efforts. In this context, we propose an automatic method for detecting trees using LiDAR data collected by airborne platforms. The proposed strategy uses the omnivariance as a key attribute, which is estimated locally from eigenvalues. Additionally, it utilizes an adaptive process to determine the optimal radius, followed by successive filtering based on the majority filter and mathematical morphology operators. The effectiveness of the proposed approach was evaluated on six study areas from two distinct datasets (Presidente Prudente/Brazil and Palmerston/New Zealand). In general, the results indicate a completeness rate around 99% and a correctness rate around 91%, resulting in an average F_{score} of 95%. These findings suggest that the proposed approach has potential to detect trees in urban regions using airborne LiDAR data. Compared to related works, the proposed strategy tends to have a better result in terms of completeness.

1. Introduction

The automation of urban forest inventories plays a crucial role in the planning and ecological management of urban environments. In this context, cartographic mapping assisted by remote sensing data is a valuable tool for promoting the sustainable development of these environments (Hecht et al., 2008; Gupta et al., 2020). Urban forests contribute significantly to the aesthetics of the landscape and mitigating ecological problems, such as reducing the local temperature of the earth's surface and atmospheric pollution, for example (Zhang et al., 2015; K. Wang et al., 2018).

Several studies have used remote sensing data collected by different platforms, such as satellite, aerial or UAV (unmanned aerial vehicles) imagery, and LiDAR (Light Detection and Ranging) data, for a wide range of applications associated with urban forests (Yan et al., 2015). Due to the increasing availability of LiDAR technology, point cloud generated by laser scanning systems have gained significant attention (Fekete and Cserep, 2021). Unlike optical data, LiDAR data is unaffected by variations in lighting conditions. Additionally, LiDAR data offers high geometric quality since the 3D point cloud is obtained directly from the integration of sensors such as laser scanning unit, Global Navigation Satellite System (GNNS) and Inertial Measurement Unit (IMU). This enables the generation of a point cloud with high positional quality, allowing the precise extraction of geometric parameters such as tree height, base height, crown depth, crown diameter (Secord and Zakhor, 2007; Hecht et al., 2008; Zhang et al., 2015), as well as the possibility of estimating biomass and carbon stock. For these and other purposes, the stage of tree detection points is essential.

These strategies can be divided into two main classes: machine learning-based and geometry-based approaches (Hui et al., 2021). Machine learning-based approaches are usually powerful (Weinmann et al., 2015; Niemeyer et al., 2016; Chen et al., 2021), but their performance can be susceptible to incorrect information in the data or insufficient training sets (Z. Wang et al., 2023). The second category relies on analyzing the spatial arrangement of points in 3D space within a local neighborhood (Özdemir et al., 2021; Alencar et al., 2023). The main limitations of geometry-based approaches are usually associated with the empirical definition of parameters (local neighborhood definition and segmentation threshold selection).

Most of the approaches for the detection of trees have been developed for applications in the forest environment (Gupta et al., 2020). Zhang et al. (2015) consider three main challenges in using LiDAR data for urban forest inventories: the complexity of urban areas, the spatial heterogeneity of the urban forest and the diversity of structure and shape of urban trees. These challenges persist, and the development of general approaches for dealing with them continue to be a source of research. In this sense, we propose an automatic tree detection based on geometric characteristics. The main contributions of this work are the following:

i) The detection of tree points directly on the original point cloud;
ii) The use of the optimal neighborhood concept to calculate ominivariance and the intuitive definition of thresholds/parameters based on geometric characteristics of trees (crown area) and in the sampling rate of the available point cloud (point density and average point spacing);
iii) Proposal of a refinement strategy based on majority filter (MF) and mathematical morphology (MM) to improve the classification results.

This contribution has been peer-reviewed. The double-blind peer-review was conducted on the basis of the full paper.
https://doi.org/10.5194/isprs-annals-X-3-2024-109-2024 | © Author(s) 2024. CC BY 4.0 License.

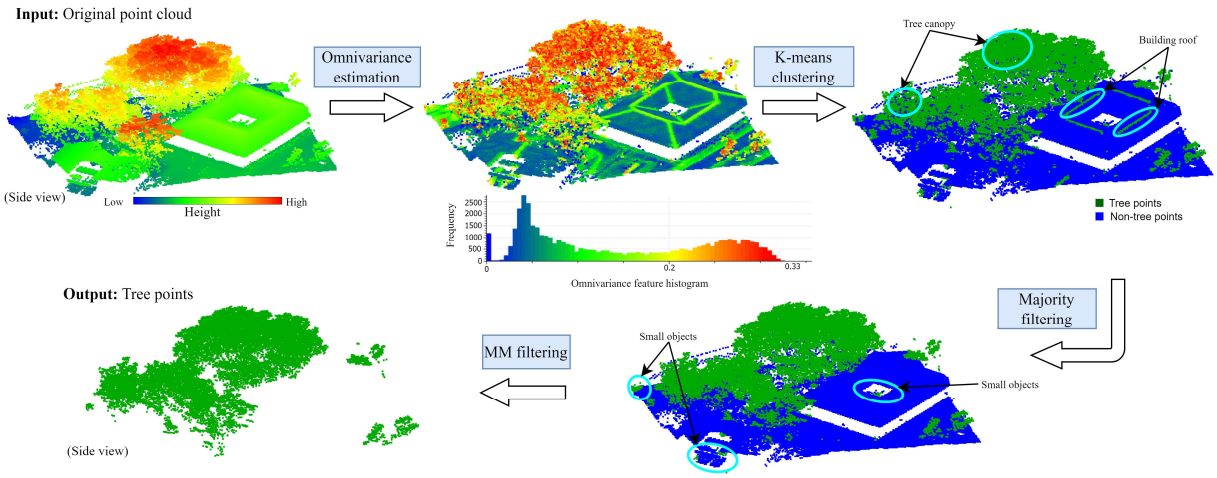

Figure 1 - Proposed approach for automatic tree detection.

2. Tree Detection Approach

Figure 1 illustrate the proposed workflow for the automatic tree detection. It is divided into four main stages: estimation of the omnivariance attribute for each point based on the eigenvalues, using an optimal neighborhood; identification of potential tree points through K-means clustering; filtering based on the majority filter; and filtering guided by mathematical morphology. The input data is the original point cloud, whereas the output data corresponds to the points classified as tree.

2.1 Geometric Feature Estimation and Tree Point Classification

2.1.1 Omnivariance Feature and Optimal Local Neighborhood

According to West et al. (2004), omnivariance feature can be estimated from eigenvalues (λ_1, λ_2, λ_3) (Equation 1), with $\lambda_1 \geq \lambda_2 \geq \lambda_3 \geq 0$. These eigenvalues are derived from the local 3D variance-covariance matrix, which describes how points spread around the local neighborhood of a given point i (dos Santos et al., 2022; Weinmann et al., 2014, 2017).

$$O_{\lambda_i} = \sqrt[3]{\lambda_1 \lambda_2 \lambda_3} \quad (1)$$

This local characteristic allows tree points to be distinguished from other objects (dos Santos and Galo, 2021, 2024; Weinmann et al., 2017). As can be seen in Figure 1, points sampled on trees tend to have higher omnivariance values, whereas points sampled on building roofs tend to have lower values.

In 3D point cloud processing, the neighborhood (N_i) of a generic point p_i can be defined by number of adjacent points around p_i, or by one sphere of radius r. In our work, a spherical neighborhood is utilized. To provide a more accurate local geometric description, we established a sphere with an adaptive radius (r^*) centered on the point p_i. The multiples neighborhood sizes are denoted by $r_1, r_2, r_3,\ldots,r_m$, ranging from r_{min} to r_{max}. The increment of each radius is represented by Δr.

The optimal neighborhood size (r^*) is automatically obtained by using the entropy concept (Weinmann et al., 2014, 2015). This metric assesses the order/disorder of points within a local neighborhood and is estimated from the eigenvalues λ_1, λ_2, and λ_3 (Equation 2).

$$E_{\lambda\, i,r} = -\lambda_1 ln(\lambda_1) - \lambda_2 ln(\lambda_2) - \lambda_3 ln(\lambda_3) \quad (2)$$

The optimal r^* is selected from Equation 3, where a minimum disorder is favored by minimizing the estimated entropy E_λ across multiples scales.

$$r_i^* = argmin\,(E_{\lambda\, i,r}),\ r \in \{r_1, r_2, r_3, \ldots, r_m\} \quad (3)$$

where $r_1 = r_{min}$, $r_2 = r_1 + \Delta r$, $r_3 = r_2 + \Delta r$, ..., $r_m = r_{max}$

2.1.2 Classification using K-means

According to previous studies (dos Santos, Galo, and Tachibana 2018; dos Santos et al. 2019; dos Santos, Galo, and Habib 2022), K-means clustering has been shown to be an effective method for LiDAR point classification when dealing with a small number of classes. In our work, we assume two main categories ($K=2$): tree and non-tree points. Then, K-means clustering establishes the optimal separation between these two classes by analyzing the omnivariance feature (Johnson and Wichern, 2007).

2.2 Tree Detection Refinement

2.2.1 Majority Filtering

Since neighboring points have a high probability of belonging to the same object, we use majority filtering (MF) to deal with classification inconsistencies.

Although this filtering approach is typically used for noise reduction in images (Shokirov et al., 2021), we adapted the MF to be applied to 3D point clouds. First, a local neighborhood is defined by a sphere of radius r_{MF} centered on a point of interest, where r_{MF} is equal to r_{max}. Next, the predominant class within this local neighborhood is then assigned to the evaluated point.

2.2.2 Mathematical Morphology-Guided Filtering

The final refinement is divided into four main steps: grid generation; median filter application; MM filtering; and 3D point cloud refinement. In the first step, a 2D grid is created along the XY plane from the potential tree points resulting from MF. The average point spacing (ps_{avg}) is used as the size of each grid cell (s_{grid}). A cell becomes active (assigns the value “1”) when it

contains at least one potential tree point, otherwise it remains inactive (assigns the value "0"), as illustrate in Figure 2a.

In the second step, a median filter (*ws* x *ws*) is applied for sparse noise reduction and elimination. In third step, the refined image is then derived from the morphological opening filter (Figure 2b). This operation involves eroding and dilating the input image using a predefined structuring element (*se*). Assuming that in general each canopy has a circular shape, we have chosen a disk as a shape for the structuring element.

In the final step, non-tree points are removed from the point cloud using the refined image as a guide. This stage is denoted as Mathematical Morphology-Guided refinement/filtering, or simply MM-guided filtering. For all potential tree points, it is checked if there is a corresponding active cell in the refined image. A planimetric distance threshold (t_{xy}) is utilized to define a valid classification, i.e., if the criterion is met, the point is retained in the cloud as a tree point; otherwise, it is labeled as a non-tree point. Figures 2c and 2d illustrated the tree points (top view) before and after MM-guided filtering.

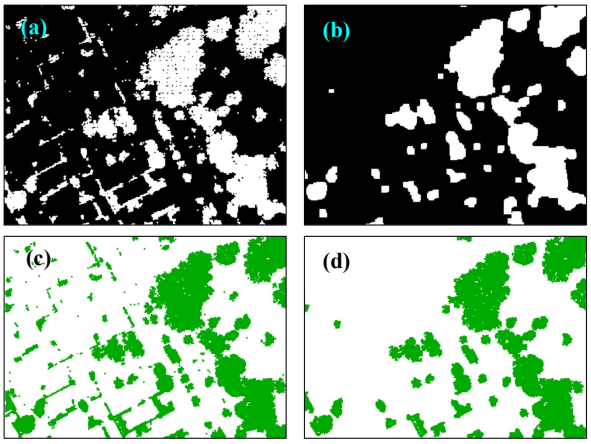

Figure 2 - Illustration of MM filtering effects on potential tree points (top view). 2D grid generated from tree candidate points (a), refined grid resulting from morphological opening filtering (b). Tree points before (c) and after (d) MM-guided filtering.

3. Experiment Design and Quality Assessment

3.1 Study Areas and Datasets

To evaluate the proposed approach in regions with distinct characteristics, six study areas located in two different countries (Figure 3) were utilized in the experiments. These areas are situated within urban regions, comprising a variety of objects (cars, buildings, trees, walls, undergrowth, power lines, and ground). In addition, the selected areas have trees with different geometric characteristics in terms of size, height, shape, and foliage density.

Table 1 provides details on each dataset, including the assigned names, study area ID, scanning system used in data collection, flying altitude, average point spacing (avg. pt. spa.), and average point density (avg. pt. den.). For clarity and ease of reference, the datasets were named according to their respective locations: Presidente Prudente/Brazil dataset (Tommaselli et al., 2018), and Palmerston/New Zealand dataset (Open Topography, n.d.). It is important to mention that the Presidente Prudente/Brazil dataset was originally captured at different flight altitudes (550 m, 900 m, 1330 m), generating clouds with different densities (12, 6 and 3 points/m^2) and average point spacing (0.4 m, 0.5 m, and 0.6 m), respectively.

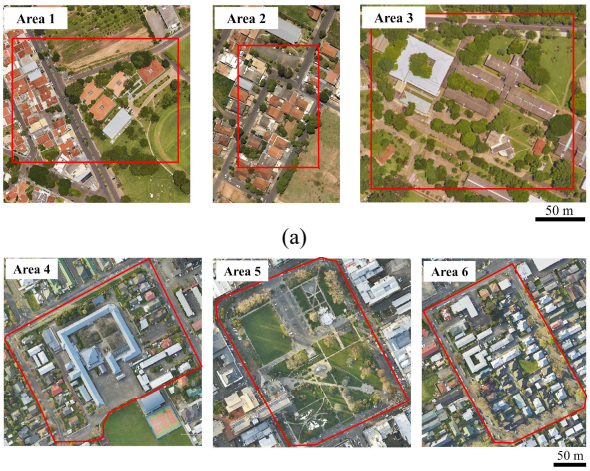

Figure 3 - Study areas. Presidente Prudente/Brazil (a) and Palmerston/New Zealand (b).

Information on data collection	Datasets	
	Presidente Prudente/Brazil	Palmerston/New Zealand
Study areas	1, 2, 3	4, 5, 6
Scanning system	RIEGL LMS-Q680i	Orion H300
Flying height (m)	550	-
Avg. pt. spa. (m)	0.4	
Avg. pt. den. (points/m^2)	12	22

Table 1 - Information on data collection and airborne LiDAR dataset characteristics.

3.2 Quality Assessment

Qualitative and quantitative analysis were performed to evaluate the performance of the proposed approach. In this stage, the detection results were compared to manually generated reference building maps.

Quantitative analysis was conducted using the following quality metrics: completeness (*Comp.*), correctness (*Corr.*), and F_{score} (Wiedemann et al., 1998; Sokolova et al., 2006). These metrics range from 0 to 1, with values closer to 1 indicating a high degree of agreement between the results and reference. In our paper, we represent these quality metrics as percentages, ranging from 0% to 100%.

$$Comp. = TP/(TP + FN) \quad (4)$$

$$Corr. = TP/(TP + FP) \quad (5)$$

$$F_{score} = 2\,TP/(2\,TP + FP + FN) \quad (6)$$

A XY-distance threshold was adopted to compute the numbers of true positive (*TP*), false positive (*FP*), and false negative (*FN*). If the distance between the detected and reference point is smaller than the pre-defined threshold, they are assumed to be a valid pair, i.e., a *TP*. In this work, the XY-distance threshold was set to the average point distance within the corresponding point cloud.

3.3 Selection of Thresholds/Parameters

The recommendations for the prediction and the adopted values for the thresholds are listed in Table 2. Most part of the thresholds can be set intuitively estimated from a superficial knowledge of the dataset, i.e., average point distance and point density, and also on the geometry of the tree of interest, i.e., the minimum size of the canopy.

4. Results

Figure 4 illustrates the results derived from the proposed approach for the selected areas (Areas 1-6). To facilitate the visualization, the results were superimposed on the original point cloud (colorized according to its intensity). In this representation, the detected tree points are associated to the green color. In addition, Figure 5 illustrates some commission errors (red arrows) and omission errors (blue arrows).

Thresholds/Parameters, with unit	Recommendations for prediction	Adopted values
r_{min} (m)	Should contain enough points for meaningful definition of the 3D structure tensor. Depends on point spacing	2 ps_{avg}*
r_{max} (m)	Depends on the size of the object of interest and/or point spacing	4 ps_{avg}
Δr (m)	Depends on the number of multiple local neighborhoods to be tested	0.1
r_{MF} (m)	Based on the maximum neighborhood used	$r_{MF} = r_{max}$
s_{grid} (m)	Depends on point spacing	$s_{grid} = ps_{avg}$
se (pixels)	Based on the smallest canopy to be detected	radius disk (2 pixels = 2 ps_{avg})
ws (pixels)	Empirically defined	3x3 pixels
t_{xy} (m)	Depends on point spacing	$t_{xy} = 2\ ps_{avg}$

* ps_{avg} - Average point spacing

Table 2 - Recommendations for the prediction and the adopted values for the thresholds.

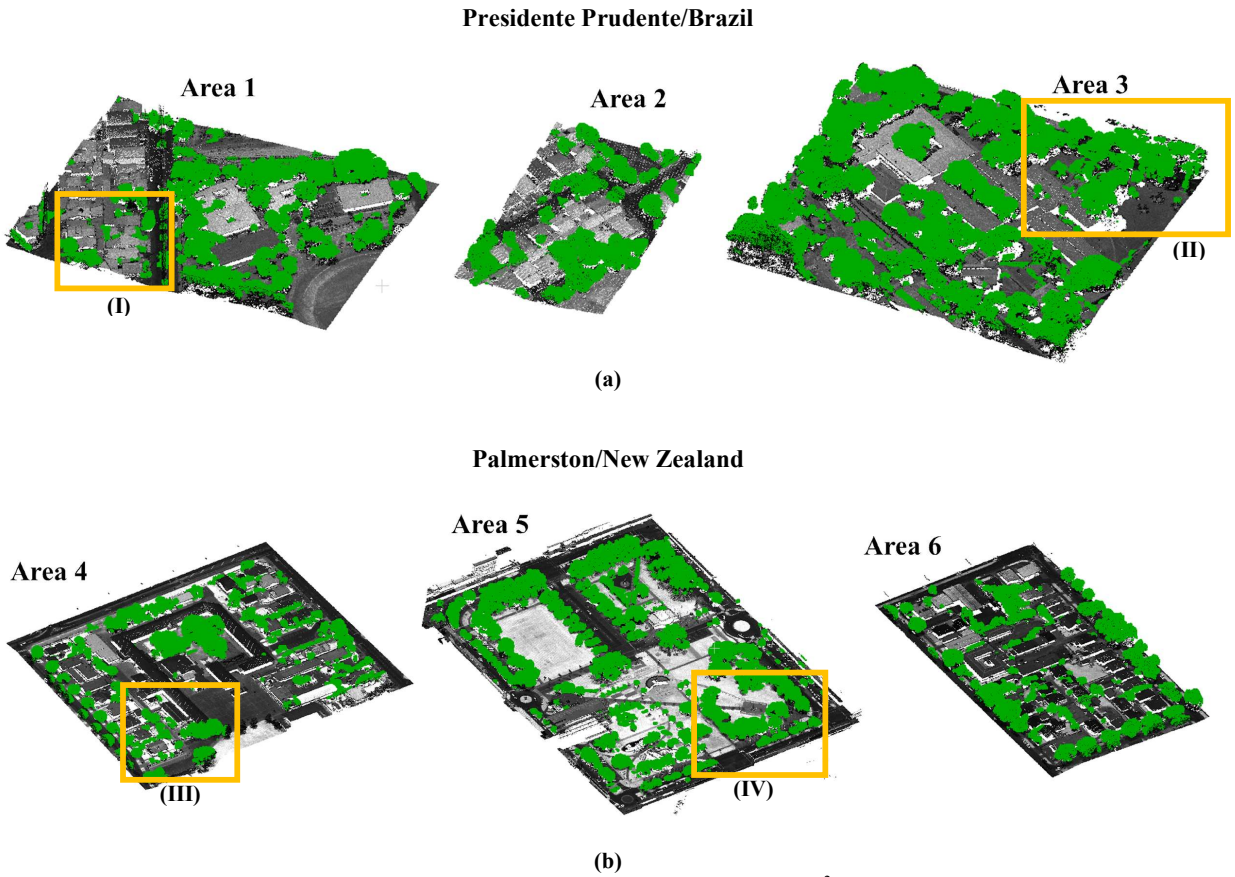

Figure 4 - Tree detection results for both datasets. Presidente Prudente/Brazil (12 points/m^2) (a) and Palmerston/New Zealand dataset (22 points/m^2) (b). Tree points (green) are displayed on the original point cloud (colored according to intensity).

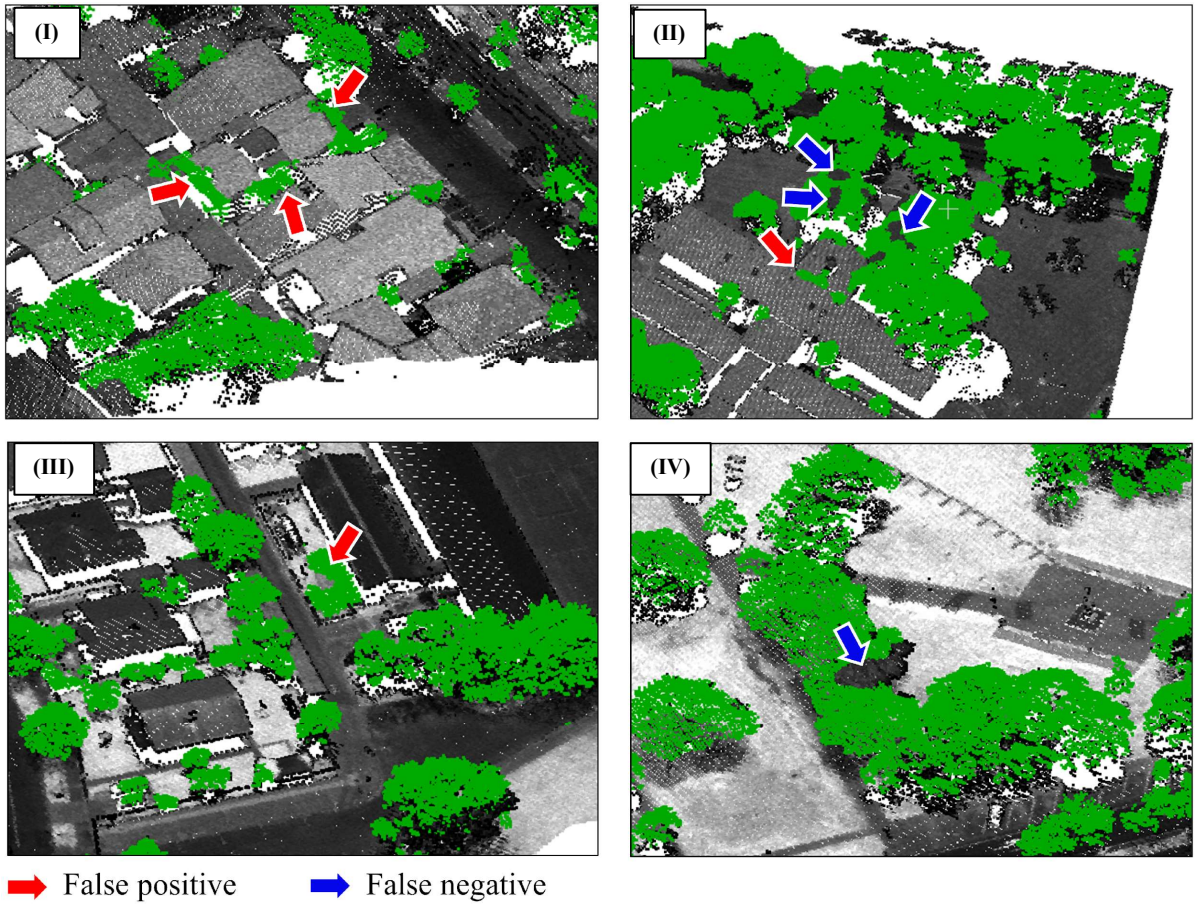

Figure 5 - Illustration of commission (false positive) and omission (false negative) errors.

Aiming to analyze the impact of point density, we show the quality metrics for Area 1 (Presidente Prudente/Brazil) for different point densities (3 points/m^2, 6 points/m^2, and 12 points/m^2), as illustrated in Figure 6.

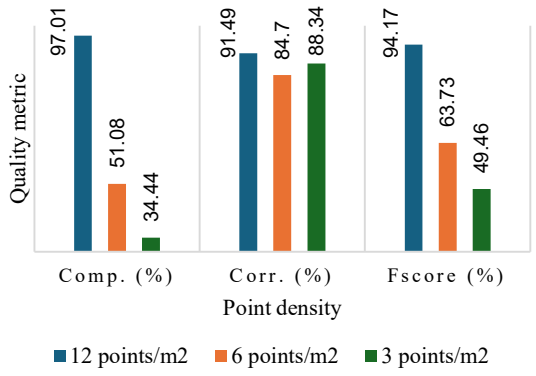

Figure 6 - Quality metrics for Area 1 for point clouds with different point densities.

As can be seen in Figure 6, although the correctness is high for all densities considered, the completeness, and consequently the F_{score}, are low for densities of 6 and 3 points/m^2, indicating that the better quality corresponds to the 12 points/m^2 density.

Table 3 lists the quality metrics estimated for all study areas, as well as the average for each dataset. It should be noted that Table 3 shows the quality metrics of the Prudente Prudente/Brazil dataset with the highest density (12 points/m^2).

	Presidente Prudente/Brazil dataset (12 points/m^2)		
Study areas	*Comp. (%)*	*Corr. (%)*	*F_{score} (%)*
Area 1	97.01	91.49	94.17
Area 2	98.84	83.94	90.78
Area 3	98.64	96.32	97.47
Mean	98.16	90.58	94.14
	Palmerston/New Zealand dataset (22 points/m^2)		
Study areas	*Comp. (%)*	*Corr. (%)*	*F_{score} (%)*
Area 4	99.35	87.27	92.92
Area 5	99.41	94.40	96.84
Area 6	98.99	93.89	96.37
Mean	99.25	91.85	95.38

Table 3 - Quality metrics estimated for study areas.

5. Discussion

Based on the visual analysis, it is possible to observe that the proposed approach produced consistent results since most of the trees were detected. However, some inconsistencies occur as

illustrated in Figure 5, which are related to commission and omission errors, affecting the quality metrics (Table 3).

Regarding to the quality metrics (Table 3), it can be noticed that the proposed approach tends to produce better results in terms of completeness (around 99%), indicating a low occurrence of omission errors (around 1%). In terms of correctness, the proposed approach shows average value around 91%, which indicates commission error rate around 9%. In addition, the results obtained in different urban areas and with different data sets were similar, indicating the robustness of the approach.

Conducting a comparative analysis for different densities, as shown in Figure 6, we can observe that the proposed method is directly impacted by the point density. In general, it tends to result in better metric parameters for point clouds with higher point density. In addition, a decrease in point density has a greater impact on the completeness metric, having a significant increase in omission errors. In general, the proposed method is suitable for datasets with a point density greater than 12 points/m^2. However, it presents limitation for datasets with lower point density (less than 6 points/m^2). These results indicated the impact of point density in tree detection.

Comparing the obtained metrics with those found in the literature, as shown in Table 4, it is possible to conclude that the proposed approach is found to be consistent with similar works. These results indicate the potential of the proposed approach for automatic tree detection in urban environments.

Approaches	**Data**	**Strategy considered by the authors**	**Type of detection**	**Point density used in the experiments (points/m^2)**	**Quality metrics**		
					Comp. (%)	*Corr. (%)*	*F_{score} (%)*
Niemeyer et al. (2016)	Airborne LiDAR data	Conditional Random Field	Supervised	≈ 8	95.1	95.9	95.5
Chen et al. (2021)	Airborne LiDAR data and optical imagery	Deep convolutional neural network (DCNN) and the 3D deep neural network (DNN)		≈ 8	80.7	85.5	83.0
Özdemir et al. (2021)	Airborne LiDAR data	Geometric characteristics	Unsupervised	≈ 8	86.8	93.1	89.8
Alencar et al. (2023)				≈ 12	92.5	73.5	81.9
Our approach				up to 12	98.7	91.2	94.8

Table 4 - Quality metrics for related works and our approach.

6. Conclusions

This paper proposes a geometry-based approach for identifying trees from airborne LiDAR point clouds. Conducted experiments indicates the potential of proposed strategy in different urban environments, presenting F_{score} around 95%. In addition, the strategy had a better performance in terms of completeness, indicating a low occurrence of omission errors. However, a drawback of this approach is its limited performance to detect trees in datasets with low point density (less than 6 points/m^2). For future investigations and aiming to broaden the applicability of the proposed approach and also to validate its efficacy across diverse scenarios, we suggest using other datasets (terrestrial LiDAR data and photogrammetric point clouds); and consider different environments, such as natural and plantation forests.

Acknowledgements

Sensormap Geotecnologia for providing the LiDAR data from Presidente Prudente/Brazil; and OpenTopography for providing the Palmerston/New Zealand dataset. The authors are also grateful to São Paulo Research Foundation - FAPESP (grant no. 2021/06029-7) and National Council for Scientific and Technological Development - CNPq (grant nº. 309734/2022-3).

References

Alencar, C. J., Galo, M., Santos, R. C. dos., 2023. Uso de descritores 3D e intensidade na detecção de árvores em ambiente urbano por meio de dados LiDAR. *Revista Brasileira de Cartografia*, *75*. https://doi.org/10.14393/rbcv75n0a-63073

Chen, Y., Liu, X., Xiao, Y., Zhao, Q., Wan, S., 2021. Three-dimensional urban land cover classification by prior-level fusion of LiDAR point cloud and optical imagery. *Remote Sensing*, *13*(23), 4928. https://doi.org/10.3390/rs13234928

dos Santos, R. C., Galo, M., 2024. Robust Building Detection in Urban Environments from Airborne LiDAR Data: A Geometry-Based Approach. *IEEE Journal of Selected Topics in Applied Earth Observations and Remote Sensing*, 17, 9429–9441. https://doi.org/10.1109/JSTARS.2024.3391050

dos Santos, R. C., Galo, M., Carrilho, A. C., Pessoa, G. G., 2021. The use of Otsu algorithm and multi-temporal airborne LiDAR data to detect building changes in urban space. *Applied Geomatics*. doi.org/10.1007/s12518-021-00371-6

dos Santos, R. C., Galo, M., Habib, A. F., 2022. K-means clustering based on omnivariance attribute for building detection from airborne LiDAR data. *ISPRS Annals of the Photogrammetry, Remote Sensing and Spatial Information Sciences*, *V-2–2022*, 111–118. doi.org/10.5194/isprs-annals-V-2-2022-111-2022

dos Santos, R. C., Galo, M., Tachibana, V. M., 2018. Classification of LiDAR data over building roofs using k-means and principal component analysis. *Boletim de Ciencias Geodesicas*, *24*(1), Article 1. doi.org/10.1590/S1982-21702018000100006

dos Santos, R. C., Pessoa, G. G., Carrilho, A. C., Galo, M., 2019. Building detection from LiDAR data using entropy and the K-means concept. *ISPRS - International Archives of the Photogrammetry, Remote Sensing and Spatial Information Sciences*, *XLII-2/W13*, 969–974. doi.org/10.5194/isprs-archives-XLII-2-W13-969-2019

Fekete, A., Cserep, M., 2021. Tree segmentation and change detection of large urban areas based on airborne LiDAR. *Computers & Geosciences*, *156*, 104900. doi.org/10.1016/j.cageo.2021.104900

Gupta, A., Byrne, J., Moloney, D., Watson, S., Yin, H., 2020. Tree annotations in lidar data using point densities and convolutional neural networks. *IEEE Transactions on Geoscience and Remote Sensing*, *58*(2), 971–981. doi.org/10.1109/TGRS.2019.2942201

Hecht, R., Meinel, G., Buchroithner, M. F., 2008. Estimation of urban green volume based on single-pulse LiDAR data. *IEEE Transactions on Geoscience and Remote Sensing*, *46*(11), 3832–3840. doi.org/10.1109/TGRS.2008.2001771

Hui, Z., Li, Z., Cheng, P., Ziggah, Y. Y., Fan, J., 2021. Building extraction from airborne LiDAR data based on multi-constraints graph segmentation. *Remote Sensing*, *13*(18), 3766. doi.org/10.3390/rs13183766

Niemeyer, J., Rottensteiner, F., Soergel, U., Heipke, C., 2016. Hierarchical higher order CRF for the classification of airborne LiDAR point clouds in urban areas. *ISPRS - International Archives of the Photogrammetry, Remote Sensing and Spatial Information Sciences*, *XLI-B3*, 655–662. doi.org/10.5194/isprsarchives-XLI-B3-655-2016

Open Topography. (n.d.). *Palmerston/New Zealand Dataset—Open Topography, High-Resolution Topography Data and Tools*. Retrieved December 28, 2021, from https://portal.opentopography.org/login

Özdemir, S., Akbulut, Z., Karsli, F., Acar, H., 2021. Automatic extraction of trees by using multiple return properties of the lidar point cloud. *International Journal of Engineering and Geosciences*, *6*(1), 20–26. doi.org/10.26833/ijeg.668352

R. A Johnson, Wichern, D. W., 2007. *Applied multivariate statistical analysis*. Upper Saddle River, NJ: Pearson Prentice Hall.

Secord, J., Zakhor, A., 2007. Tree detection in urban regions using aerial LiDAR and image data. *IEEE Geoscience and Remote Sensing Letters*, *4*(2), 196–200. doi.org/10.1109/LGRS.2006.888107

Shokirov, S., Schaefer, M., Levick, S. R., Jucker, T., Borevitz, J., Abdurahmanov, I., Youngentob, K., 2021. Multi-platform LiDAR approach for detecting coarse woody debris in a landscape with varied ground cover. *International Journal of Remote Sensing*, *42*(24), 9324–9350. doi.org/10.1080/01431161.2021.1995072

Sokolova, M., Japkowicz, N., Szpakowicz, S., 2006. Beyond accuracy, F-Score and ROC: a family of discriminant measures for performance evaluation. Sattar A., Kang B. (eds) AI 2006: Advances in Artificial Intelligence. AI 2006. Lecture Notes in Computer Science, 4304. Springer, Berlin, Heidelberg. doi.org/ 10.1007/11941439_114.

Tommaselli, A. M. G., Galo, M., Dos Reis, T. T., Ruy, R. da S., Moraes, M. V. A., Matricardi, W. V., 2018. Development and assessment of a data set containing frame images and dense airborne laser scanning point clouds. *IEEE Geoscience and Remote Sensing Letters*, *15*(2), Article 2. https://doi.org/10.1109/lgrs.2017.2779559

Wang, K., Wang, T., Liu, X., 2018. A review: individual tree species classification using integrated airborne LiDAR and optical imagery with a focus on the urban environment. *Forests*, *10*(1), 1. doi.org/10.3390/f10010001

Wang, Z., Li, P., Cui, Y., Lei, S., Kang, Z., 2023. Automatic detection of individual trees in forests based on airborne LiDAR data with a tree region-based convolutional neural network (RCNN). *Remote Sensing*, *15*(4), 1024. doi.org/10.3390/rs15041024

Weinmann, M., Jutzi, B., Hinz, S., Mallet, C., 2015. Semantic point cloud interpretation based on optimal neighborhoods, relevant features and efficient classifiers. *ISPRS Journal of Photogrammetry and Remote Sensing*, *105*, 286–304. doi.org/10.1016/j.isprsjprs.2015.01.016

Weinmann, M., Jutzi, B., Mallet, C., 2014. Semantic 3D scene interpretation: A framework combining optimal neighborhood size selection with relevant features. *ISPRS Annals of the Photogrammetry, Remote Sensing and Spatial Information Sciences*, *II–3*, 181–188. doi.org/10.5194/isprsannals-II-3-181-2014

Weinmann, M., Jutzi, B., Mallet, C., Weinmann, M., 2017. Geometric features and their relevance for 3D point cloud classification. *ISPRS Annals of the Photogrammetry, Remote Sensing and Spatial Information Sciences*, *IV-1-W1*, 157–164. doi.org/10.5194/isprs-annals-IV-1-W1-157-2017

West, K. F., Webb, B. N., Lersch, J. R., Pothier, S., Triscari, J. M., Iverson, A. E., 2004. *Context-driven automated target detection in 3D data* (F. A. Sadjadi, Ed.; pp. 133–143). doi.org/10.1117/12.542536

Wiedemann, C., Heipke, C., Mayer, H., Jamet, O., 1998. Empirical evaluation of automatically extracted road axes. In K. W. Bowyer and P. J. Phillips (Eds.), *Empirical evaluation techniques in computer vision* (pp. 172–187). Wiley-IEEE Computer Society Press.

Yan, W. Y., Shaker, A., El-Ashmawy, N., 2015. Urban land cover classification using airborne LiDAR data: A review. *Remote Sensing of Environment*, *158*, 295–310. doi.org/10.1016/j.rse.2014.11.001

Zhang, C., Zhou, Y., Qiu, F., 2015. Individual tree segmentation from LiDAR point clouds for urban forest inventory. *Remote Sensing*, *7*(6), 7892–7913. doi.org/10.3390/rs70607892